

## Article

# Antibacterial Ingredients and Modes of the Methanol-Phase Extract from the Fruit of *Amomum villosum* Lour.

Kaiyue Zhang <sup>1,2</sup>, Fengfeng Cao <sup>1,2</sup>, Yueliang Zhao <sup>1,2</sup>, Hengbin Wang <sup>3</sup>  and Lanming Chen <sup>1,2,\*</sup>

- <sup>1</sup> Key Laboratory of Quality and Safety Risk Assessment for Aquatic Products on Storage and Preservation, Ministry of Agriculture and Rural Affairs of the People's Republic of China, Shanghai 201306, China
- <sup>2</sup> College of Food Science and Technology, Shanghai Ocean University, Shanghai 201306, China
- <sup>3</sup> Department of Internal Medicine, Division of Hematology, Oncology, and Palliative Care, Massey Cancer Center, School of Medicine, Virginia Commonwealth University, Richmond, VA 23298, USA
- \* Correspondence: lmchen@shou.edu.cn

**Abstract:** Epidemics of infectious diseases threaten human health and society stability. Pharmacophagous plants are rich in bioactive compounds that constitute a safe drug library for antimicrobial agents. In this study, we have deciphered for the first time antibacterial ingredients and modes of the methanol-phase extract (MPE) from the fruit of *Amomum villosum* Lour. The results have revealed that the antibacterial rate of the MPE was 63.64%, targeting 22 species of common pathogenic bacteria. The MPE was further purified by high performance liquid chromatography (Prep-HPLC), and three different constituents (Fractions 1–3) were obtained. Of these, the Fraction 2 treatment significantly increased the cell membrane fluidity and permeability, reduced the cell surface hydrophobicity, and damaged the integrity of the cell structure, leading to the leakage of cellular macromolecules of Gram-positive and Gram-negative pathogens ( $p < 0.05$ ). Eighty-nine compounds in Fraction 2 were identified by ultra HPLC-mass spectrometry (UHPLC-MS) analysis, among which 4-hydroxyphenylacetylglutamic acid accounted for the highest 30.89%, followed by lubiprostone (11.86%), miltirone (10.68%), and oleic acid (10.58%). Comparative transcriptomics analysis revealed significantly altered metabolic pathways in the representative pathogens treated by Fraction 2 ( $p < 0.05$ ), indicating multiple antibacterial modes. Overall, this study first demonstrates the antibacterial activity of the MPE from the fruit of *A. villosum* Lour., and should be useful for its application in the medicinal and food preservative industries against common pathogens.

**Keywords:** *Amomum villosum* Lour.; antibacterial compound; antibacterial mechanism; pathogen; infectious disease; pharmacophagous plant



**Citation:** Zhang, K.; Cao, F.; Zhao, Y.; Wang, H.; Chen, L. Antibacterial Ingredients and Modes of the Methanol-Phase Extract from the Fruit of *Amomum villosum*

Lour. *Plants* **2024**, *13*, 834. <https://doi.org/10.3390/plants13060834>

Academic Editor: Adriana Basile

Received: 20 February 2024

Revised: 6 March 2024

Accepted: 6 March 2024

Published: 14 March 2024



**Copyright:** © 2024 by the authors. Licensee MDPI, Basel, Switzerland. This article is an open access article distributed under the terms and conditions of the Creative Commons Attribution (CC BY) license (<https://creativecommons.org/licenses/by/4.0/>).

## 1. Introduction

Epidemics of infectious diseases threaten human health, cause loss of life, and seriously impact the economy [1,2]. In recent decades, due to the inappropriate use of antibiotics, clinical antibiotic therapy has become increasingly ineffective in preventing outbreaks and spreading of infectious diseases [3]. Therefore, it is imperative to search for safe and effective antimicrobial alternatives. Pharmacophagous plants with safety and low toxicity properties are traditionally used to treat many diseases. These plant extracts constitute an ideal drug library for antimicrobial agents [4].

*Amomum villosum* Lour. is a comestible medicinal plant that belongs to the Zingiberaceae family. This plant is mainly distributed in the tropical regions of Asia and Oceania. Its dry fruits and seeds are often used as cooking condiments, with a unique and rich aroma, and also used as valuable traditional medicines, such as for the obstruction of body dampness and turbidity, stomach deficiency and cold, and vomiting and diarrhea [5,6]. Recent studies have provided experimental evidence for the pharmacological activities of *A. villosum* Lour., such as anti-ulcer, anti-diarrhea, and anti-inflammation [7]. For example, Yin et al. [8] reported that the extracted labdane and norlabdane diterpenoids from the

rhizomes of *A. villosum* Lour. showed anti-inflammatory and  $\alpha$ -glucosidase inhibitory activities. Luo et al. [9] reported that the dietary supplement of *A. villosum* Lour. polysaccharide attenuated ulcerative colitis of balb/c mice, a prospective nutritional strategy for the treatment of inflammatory bowel diseases.

Nevertheless, the current literature on the bacteriostasis activity of *A. villosum* Lour. is rare. To the best of our knowledge, the only other study reported that essential oil (EO) of *A. villosum* Lour. inhibited the growth of *Staphylococcus aureus* ATCC43 [10]. In order to further explore the antibacterial activity of *A. villosum* Lour., in this study, we aimed to extract bioactive compounds in the fruit of *A. villosum* Lour. using the methanol–chloroform extraction (M–CE) method, which has been well established in our laboratory [11–14], and to decipher the antibacterial ingredients and modes of the methanol-phase extract (MPE) from *A. villosum* Lour.

## 2. Results and Discussion

### 2.1. Antibacterial Activity of Crude Extracts from the Fruit of *A. villosum* Lour.

Based on our recent studies [11–14], the M–CE method was employed to extract antibacterial substances from the fruit of *A. villosum* Lour. Its water loss rate was 73.68% after freeze-drying at  $-80$  °C for 48 h. The extraction yields of the MPE and chloroform-phase extract (CPE) of *A. villosum* Lour. were 12.00% and 2.80%, respectively.

The antibacterial activities of the MPE and CPE of *A. villosum* Lour. were determined, targeting 22 species of common pathogenic bacteria. As shown in Table 1, the MPE showed an inhibition rate of 63.64% and repressed the growth of 14 species of bacteria, including the following: 2 species of Gram-positive bacteria: *S. aureus* and *Bacillus cereus*; and 12 species of Gram-negative bacteria: *Aeromonas hydrophila*, *Pseudomonas aeruginosa*, *Shigella dysenteriae*, *Shigella flexneri*, *Shigella sonnei*, *Salmonella enterica* subsp. *enterica* (ex Kauffmann and Edwards), *Vibrio alginolyticus*, *Vibrio cholerae*, *Vibrio harveyi*, *Vibrio metschnikovi*, *Vibrio mimicus*, and *Vibrio parahaemolyticus*. The CPE showed an inhibition rate of 54.55% and inhibited 1 species of Gram-positive and 11 species of Gram-negative bacteria (Table 1).

**Table 1.** Antibacterial activities of the MPE and CPE from the fruit of *A. villosum* Lour.

Bacterial Strain	DIZ (Diameter, mm)		MIC ( $\mu$ g/mL)
	MPE	CPE	MPE
<i>Aeromonas hydrophila</i> ATCC35654	8.00 $\pm$ 0.26	10.00 $\pm$ 0.53	1024
<i>Bacillus cereus</i> Y1	9.50 $\pm$ 0.26	8.00 $\pm$ 0.56	512
<i>Enterobacter cloacae</i> ATCC13047	—	8.00 $\pm$ 0.26	—
<i>Enterobacter cloacae</i> D1	—	—	—
<i>Escherichia coli</i> ATCC8739	—	8.00 $\pm$ 0.10	—
<i>Escherichia coli</i> K12	—	—	—
<i>Escherichia coli</i> ATCC25922	—	9.00 $\pm$ 0.36	—
<i>Enterobacter sakazakii</i> CMCC45401	—	—	—
<i>Klebsiella pneumoniae</i> 7-17-16	—	9.00 $\pm$ 0.44	—
<i>Pseudomonas aeruginosa</i> ATCC9027	—	8.00 $\pm$ 0.17	—
<i>Pseudomonas aeruginosa</i> ATCC27853	8.00 $\pm$ 0.36	9.00 $\pm$ 0.17	1024
<i>Staphylococcus aureus</i> GIM1.481	9.50 $\pm$ 0.20	—	512
<i>Staphylococcus aureus</i> GIM1.441	11.00 $\pm$ 0.53	—	128
<i>Staphylococcus aureus</i> GIM1.160	—	—	—
<i>Shigella dysenteriae</i> CMCC51252	9.00 $\pm$ 0.56	—	512
<i>Salmonella choleraesuis</i> ATCC13312	—	—	—
<i>Shigella flexneri</i> GIM1.238	8.50 $\pm$ 0.26	9.00 $\pm$ 0.44	1024
<i>Shigella flexneri</i> GIM1.539	—	—	—
<i>Shigella flexneri</i> GIM1.231	—	—	—

Table 1. Cont.

Bacterial Strain	DIZ (Diameter, mm)		MIC ( $\mu\text{g/mL}$ )
	MPE	CPE	MPE
<i>Salmonella paratyphi</i> GIM1.235	—	—	—
<i>Shigella sonnei</i> GIM1.424	9.00 $\pm$ 0.17	—	512
<i>Shigella sonnei</i> GIM1.239	—	9.00 $\pm$ 0.35	—
<i>Salmonella enterica</i> subsp. <i>enterica</i> (ex Kauffmann and Edwards) Le Minor and Popoff serovar Vellore ATCC15611	9.00 $\pm$ 0.17	—	512
<i>Vibrio cholerae</i> GIM1.449	8.50 $\pm$ 0.26	9.00 $\pm$ 0.52	1024
<i>Vibrio cholerae</i> B1	—	8.00 $\pm$ 0.61	—
<i>Vibrio parahaemolyticus</i> B2-28	9.50 $\pm$ 0.26	—	256
<i>Vibrio parahaemolyticus</i> N2-5	9.00 $\pm$ 0.40	—	1024
<i>Vibrio parahaemolyticus</i> N9-20	9.00 $\pm$ 0.35	—	512
<i>Vibrio alginolyticus</i> ATCC33787	8.00 $\pm$ 0.50	—	1024
<i>Vibrio fluviialis</i> ATCC33809	—	10.00 $\pm$ 0.10	—
<i>Vibrio harveyi</i> ATCC BAA-1117	8.00 $\pm$ 0.53	—	1024
<i>Vibrio harveyi</i> ATCC33842	—	10.00 $\pm$ 0.26	—
<i>Vibrio metschnikovi</i> ATCC700040	9.00 $\pm$ 0.30	—	512
<i>Vibrio mimicus</i> bio-56759	9.00 $\pm$ 0.44	—	512
<i>Vibrio parahaemolyticus</i> ATCC17802	9.00 $\pm$ 0.50	8.00 $\pm$ 0.53	512
<i>Vibrio parahaemolyticus</i> ATCC33847	9.00 $\pm$ 0.26	10.00 $\pm$ 0.44	512
<i>Vibrio vulnificus</i> ATCC27562	—	—	—

Note: CPE: chloroform-phase extract. MPE: methanol-phase extract. —: no antibacterial activity. DIZ: diameters of inhibitory zone, including the diameter of the disc (6 mm). MIC: minimum inhibitory concentration. The values are expressed as the mean  $\pm$  standard deviation (S.D.) of three parallel measurements.

Tang et al. [10] used water as a solvent to extract the EO of *A. villosum* Lour. and found its inhibitory effect on *S. aureus* ATCC43. In this study, our results indicated that the M-CE method was more effective in extracting antibacterial substances in *A. villosum* Lour. than water.

Given the higher antibacterial rate (63.64%), the MPE of *A. villosum* Lour. was subjected to further analysis in this study. The minimum inhibitory concentrations (MICs) of the MPE were determined, targeting the 14 species of pathogenic bacteria. As shown in Table 1, the MICs of the MPE ranged from 128 to 1024  $\mu\text{g/mL}$ . The most effective inhibition was observed against the Gram-positive bacterium *S. aureus* GIM1.441 and the Gram-negative bacterium *V. parahaemolyticus* B2-28, with MICs of 128  $\mu\text{g/mL}$  and 256  $\mu\text{g/mL}$ , respectively (Table 1).

## 2.2. Purification of the MPE of *A. villosum* Lour.

The MPE of *A. villosum* Lour. was prepared in large quantities using the Prep-high-performance-liquid-chromatography (Prep-HPLC) technique. As shown in Figure 1, three distinct constituents (designated as Fractions 1–3) were observed at 1.9–4.2 min when scanning at OD<sub>211</sub> for 15 min.

The antibacterial activity of the three different Fractions was further determined, and the results are presented in Table 2 and Figure 2. Fraction 2 displayed inhibitory effects on the two species of Gram-positive and eight species of Gram-negative bacteria. The diameters of the inhibitory zone (DIZ) ranged between 7 and 11.5 mm. In contrast, Fraction 1 and Fraction 3 had weak and no inhibitory effects, respectively (Table 2).

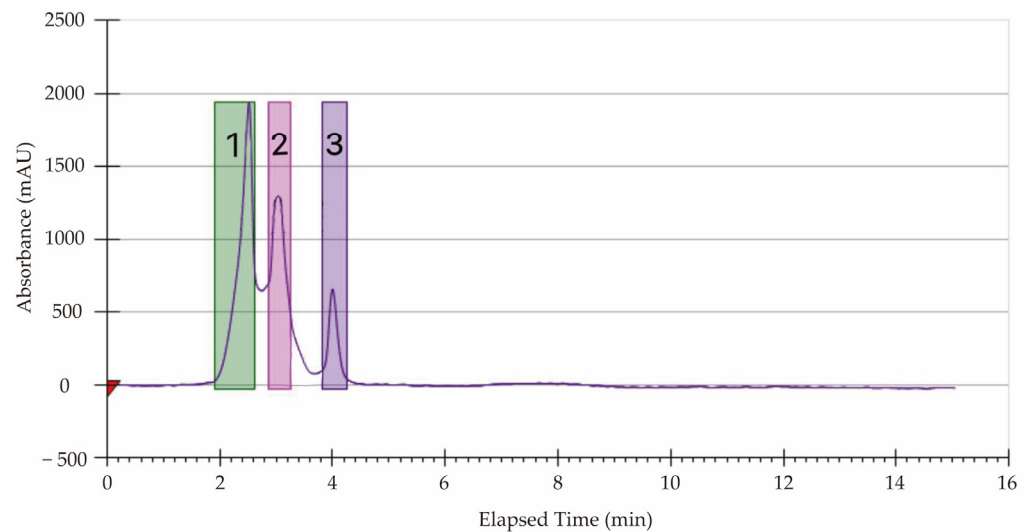


**Figure 1.** Prep-HPLC diagram of purifying the MPE from the fruit of *A. villosum* Lour. (1–3): the Fraction 1, Fraction 2, and Fraction 3, respectively.

**Table 2.** Antibacterial activities of Fraction 2 of the MPE of *A. villosum* Lour.

Bacterial Strain	DIZ (Diameter, mm)	MIC ( $\mu\text{g/mL}$ )
<i>A. hydrophila</i> ATCC35654	8.00 $\pm$ 0.44	2048
<i>B. cereus</i> Y1	11.00 $\pm$ 0.00	512
<i>S. aureus</i> GIM1.481	9.50 $\pm$ 0.15	1024
<i>S. aureus</i> GIM1.441	11.50 $\pm$ 0.26	256
<i>S. dysenteriae</i> CMCC51252	8.00 $\pm$ 0.78	2048
<i>S. flexneri</i> GIM1.238	8.00 $\pm$ 0.61	2048
<i>S. sonnei</i> GIM1.424	8.50 $\pm$ 0.1	1024
<i>Salmonella enterica</i> subsp. <i>enterica</i> (ex Kauffmann and Edwards) Le Minor and Popoff serovar Vellore ATCC15611	8.00 $\pm$ 0.35	2048
<i>V. parahemolyticus</i> B2-28	11.00 $\pm$ 0.26	512
<i>V. parahemolyticus</i> N2-5	8.00 $\pm$ 0.61	2048
<i>V. parahemolyticus</i> N9-20	7.00 $\pm$ 0.10	4096
<i>V. alginolyticus</i> ATCC33787	8.00 $\pm$ 0.36	2048
<i>V. mimicus</i> bio-56759	9.00 $\pm$ 0.56	1024
<i>V. parahemolyticus</i> ATCC17802	10.00 $\pm$ 0.26	1024
<i>V. parahemolyticus</i> ATCC33847	8.00 $\pm$ 0.46	2048

We also determined the MICs of Fraction 2. As shown in Table 2, the strongest antibacterial efficacy of Fraction 2 was observed against *S. aureus* GIM1.441, *B. cereus* Y1, and *V. parahemolyticus* B2-28, with MICs of 256  $\mu\text{g/mL}$ , 512  $\mu\text{g/mL}$ , and 512  $\mu\text{g/mL}$ , respectively, consistent with the results yielded from the MPE of *A. villosum* Lour.

The Gram-positive bacterium *S. aureus* can cause human skin and tissue infections and sepsis in severe cases [15], while *B. cereus* can cause self-limiting emetic and diarrhea diseases [16]. The Gram-negative bacterium *V. parahemolyticus* is a leading sea-food-borne pathogen worldwide, and common clinical symptoms include headache, nausea, vomiting, and diarrhea. Severe infections caused by *V. parahemolyticus* can develop into sepsis or even death [17].

In order to decipher the antibacterial mechanisms of Fraction 2 of *A. villosum* Lour., based on the above results, the Gram-positive bacteria *S. aureus* GIM1.441 and *B. cereus* Y1 and the Gram-negative bacterium *V. parahemolyticus* B2-28 were chosen as target strains for further analyses in this study.

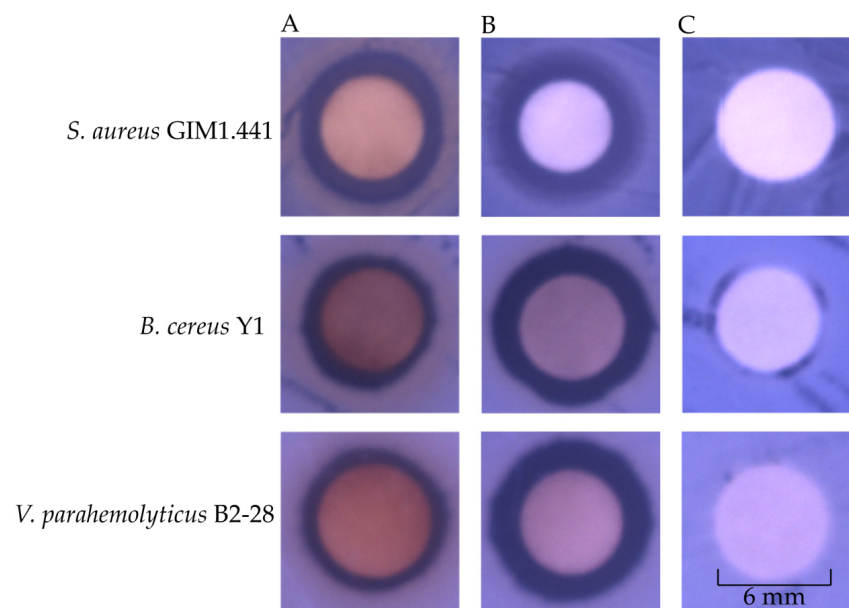


**Figure 2.** The DIZs of the MPE and Fraction 2 of MPE from *A. villosum* Lour. (A–C): the MPE, Fraction 2 of MPE, and negative control, respectively.

### 2.3. Inhibited Growth of the Target Strains Treated with Fraction 2 of *A. villosum* Lour.

We determined growth curves of the three target strains treated with Fraction 2 of *A. villosum* Lour. As shown in Figure S1, *S. aureus* GIM1.441 was strongly inhibited when incubated in tryptone soybean broth (TSB) medium supplemented with 1 × MIC of Fraction 2. The inhibition showed a concentration-dependent mode, as *S. aureus* GIM1.441 was found to grow at 1/2 × MIC of Fraction 2, but showed lower biomass (maximum OD<sub>600</sub> = 0.9065), as compared to the control group (maximum OD<sub>600</sub> = 1.205) (Figure S1A).

Similarly, the inhibition by the 1 × MIC of Fraction 2 was also stronger on *B. cereus* Y1 than the 1/2 × MIC (Figure S1B). The same case was apparent for the Gram-negative bacterium *V. parahemolyticus* B2-28, but this bacterium appeared to be the most sensitive to the Fraction 2 treatment among the test strains (Figure S1C).

Taken together, the 1 × MIC (256 µg/mL, 512 µg/mL, 512 µg/mL) of Fraction 2 was chosen as the treatment conditions for *S. aureus* GIM1.441, *B. cereus* Y1, and *V. parahemolyticus* B2-28, respectively, in the further analyses in this study.

### 2.4. Changed Cell Surface Hydrophobicity (CSH), Cell Membrane Fluidity (CMF), and Cell Membrane Permeability (CMP) of the Target Strains Treated with Fraction 2 of *A. villosum* Lour.

The interaction between microbial cells and the host is influenced by the biophysical properties of the cell membrane, such as the CSH [18]. In this study, we observed that the CSH of the target strains was remarkably reduced in all of the treatment groups after 4 h- and 6 h-treatment of Fraction 2 of *A. villosum* Lour., as compared to the control groups ( $p < 0.05$ ). Moreover, the decreased CSH of the strains was closely related to prolonged treatment time (Figure 3A). For example, after being treated with Fraction 2 for 2 h, the CSH of *S. aureus* GIM1.441 did not significantly change ( $p > 0.05$ ). However, the decreased CSH was observed to be 1.23-fold and 2.05-fold after treatment for 4 h and 6 h, respectively ( $p < 0.001$ ). Similarly, the CSH of *B. cereus* Y1 decreased by 1.07-fold to 2.56-fold after the treatment for 2 h to 6 h ( $p < 0.05$ ). The strongest decrease (2.12-fold) in the CSH was found in *V. parahaemolyticus* B2-28 after being treated with Fraction 2 for 2 h ( $p < 0.001$ ).

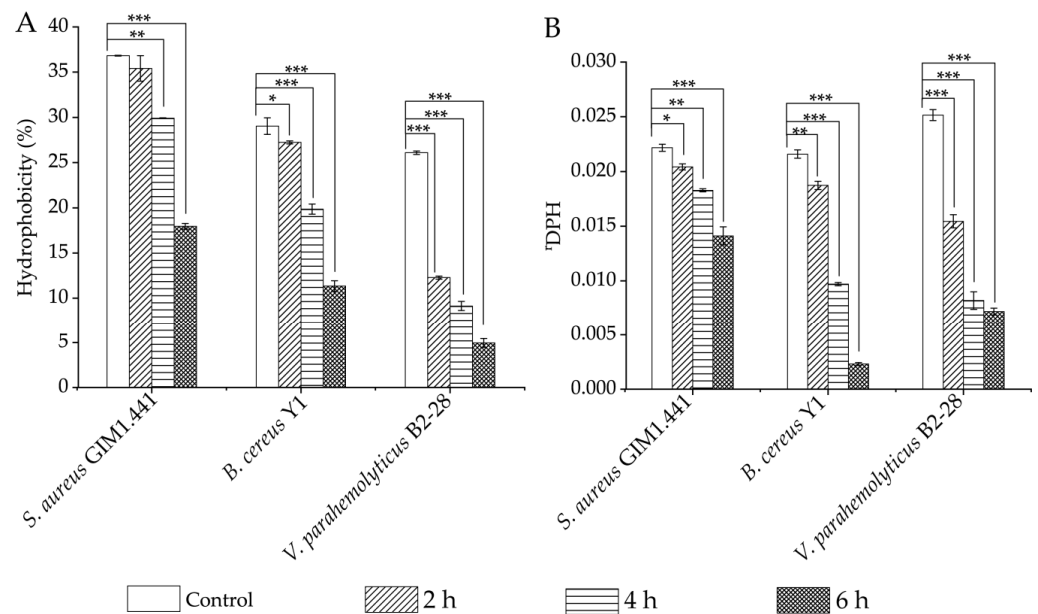


**Figure 3.** Effects of Fraction 2 (1 x MIC) of *A. villosum* Lour. on the CSH and CMF of the target strains. (A,B): CSH and CMF, respectively. \*:  $p < 0.05$ ; \*\*:  $p < 0.01$ ; \*\*\*:  $p < 0.001$ .

The CMF is also a key parameter of the bacterial cell membrane. In this study, 1,6-diphenyl-1,3,5-hexatriene (DPH) was used as a probe to detect the changes in CMF of the target strains. Higher DPH values indicated weaker CMF [19]. As shown in Figure 3B, as compared to the control groups, the CMF of the three target strains increased significantly (1.09-fold, 1.15-fold, and 1.63-fold) after being treated with Fraction 2 for 2 h ( $p < 0.05$ ). Among the three strains, the CMF of *V. parahaemolyticus* B2-28 and *B. cereus* Y1 increased the most (3.06-fold and 9.35-fold) after the 4-h- and 6-h-treatment, respectively ( $p < 0.001$ ).

The bacterial cell membrane is a permeable barrier against external harmful substances; therefore, it is the therapeutic target of antimicrobial agents [20]. In this study, the *o*-nitrophenyl- $\beta$ -D-galactopyranoside (ONPG) was used as a probe to detect the changes in the CMP of the target strains. As shown in Figure 4A, as compared to the control group, there were no significant changes in the CMP of *S. aureus* GIM1.441 after being treated with Fraction 2 of *A. villosum* Lour. for 2 h and 4 h ( $p > 0.05$ ). However, a significant increase in the CMP was observed after the 6 h-treatment ( $p < 0.05$ ). *B. cereus* Y1 showed a 1.08-fold increase in the CMP after the treatment for 2 h ( $p < 0.05$ , Figure 4B). Similarly, the increased CMP of *V. parahemolyticus* B2-28 was also observed to be 1.14-fold to 1.25-fold after being treated with Fraction 2 for 2 h to 6 h ( $p < 0.05$ , Figure 4C).

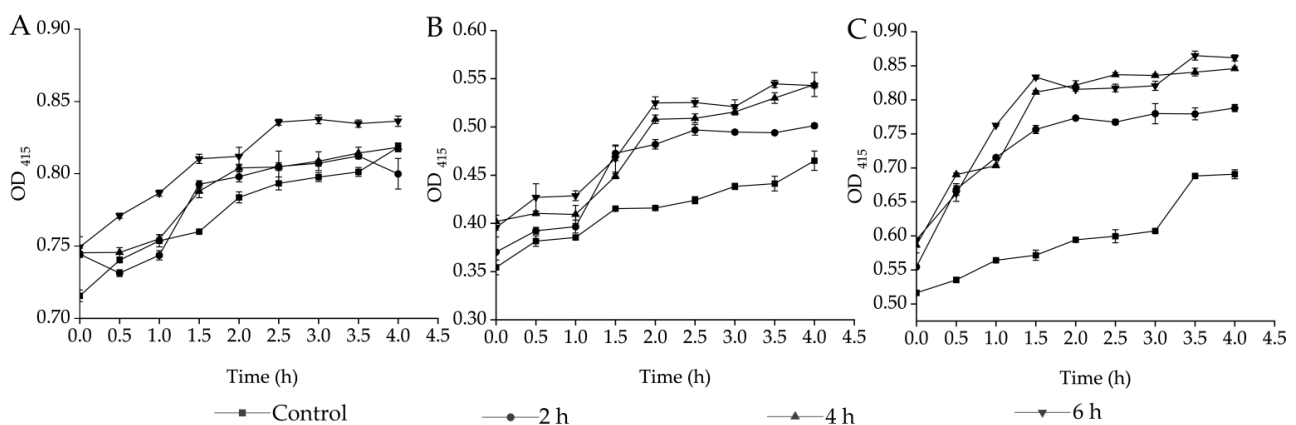


**Figure 4.** Effects of Fraction 2 of *A. villosum* Lour. on the CMP of the target strains. (A–C): *S. aureus* GIM1.441, *B. cereus* Y1, and *V. parahemolyticus* B2-28, respectively.

Taken together, the Fraction 2 treatment can significantly reduce the CSH but increase the CMP and CMF of Gram-positive *S. aureus* GIM1.441 and *B. cereus* Y1 and Gram-negative *V. parahaemolyticus* B2-28. The antibacterial effects are exerted with the treatment-time-dependent mode.

### 2.5. Changed Cell Morphological Structure of the Target Strains Treated with Fraction 2 of *A. villosum* Lour.

Based on the above results, we wondered whether the cell structure of the target strains was damaged by the Fraction 2 treatment. Therefore, we observed the cell structure changes in *S. aureus* GIM1.441, *B. cereus* Y1, and *V. parahaemolyticus* B2-28 using a scanning electron microscope (SEM). As shown in Figure 5, the bacterial cells in the control groups were intact, with a full shape and clear structure. However, in the treatment groups, the cells showed varying degrees of folds, breaks, and pores after being treated with Fraction 2 for 2 h to 6 h.

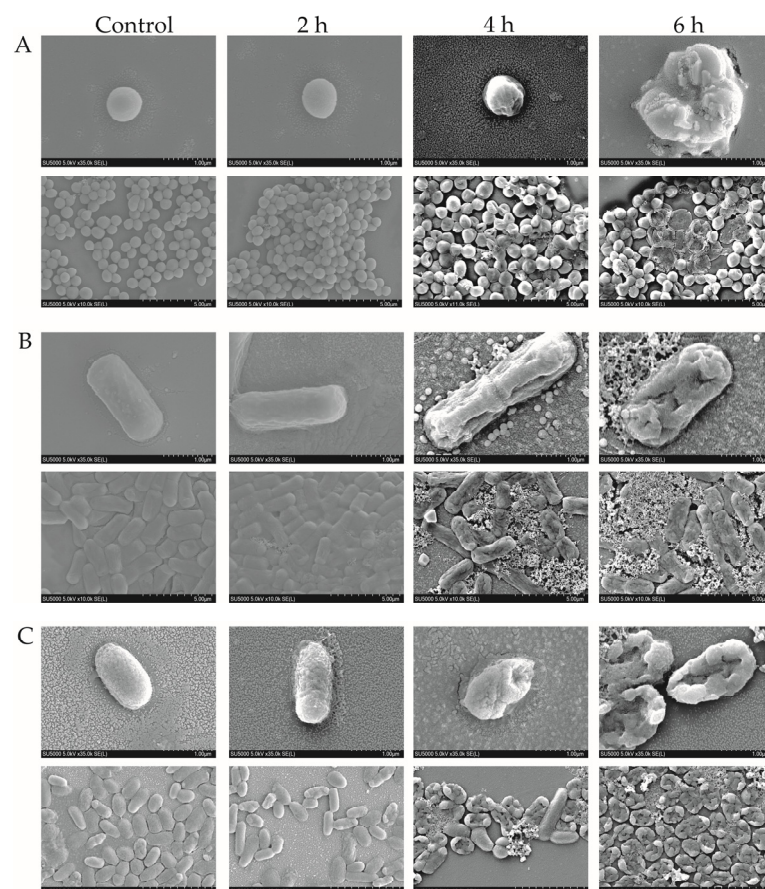


**Figure 5.** SEM observation of cell structure of the target strains treated with Fraction 2 of *A. villosum* Lour. (A–C): *S. aureus* GIM1.441, *B. cereus* Y1, and *V. parahaemolyticus* B2-28, respectively.

For example, for the Gram-positive bacterium *S. aureus* GIM1.441, no significant change in the bacterial cell surface was observed after the 2 h-treatment with Fraction 2. However, the wrinkled cell surface occurred after the 4 h-treatment, and they even burst after the 6 h-treatment (Figure 5A). A similar case was found for *B. cereus* Y1 (Figure 5B).

For the Gram-negative bacterium *V. parahaemolyticus* B2-28, severe ruffling on the cell surface, and even a wrinkled cell structure, were observed after the treatment for 2 h. Remarkably, the bacterial cells were fully ruptured after the treatment for 6 h (Figure 5C).

Tang et al. [10] reported that the surface of *S. aureus* ATCC43 appeared irregular, wrinkled, and uneven, but did not burst after being treated with the EO of *A. villosum*

Lour. for 6 h. These results have provided additional evidence to validate that the MPE of *A. villosum* Lour. has a stronger antibacterial efficacy on the target strains than the EO.

Taken together, Fraction 2 of *A. villosum* Lour. can destroy the cell structure of Gram-positive and Gram-negative bacteria to varying degrees. Moreover, the treatment is the most effective against the Gram-negative bacterium *V. parahemolyticus* B2-28.

### 2.6. Nucleotide Acid and Protein Exudation of the Target Strains Treated with Fraction 2 of *A. villosum* Lour.

Damage to the cell structure may lead to the leakage of macromolecules. Therefore, we examined the nucleotide acid and protein exudation of the target strains treated with Fraction 2 of *A. villosum* Lour. As shown in Figure 6A, as compared to the control group, the amount of nucleotide acids exuded from *S. aureus* GIM1.441 was significantly increased by 1.55-fold after being treated with Fraction 2 for 2 h ( $p < 0.001$ ). More extracellular nucleotide acids (2.22-fold and 3.18-fold) were detected with the longer treatment time (4 h and 6 h) ( $p < 0.001$ ). A similar case was observed in *B. cereus* Y1 and *V. parahaemolyticus* B2-28.

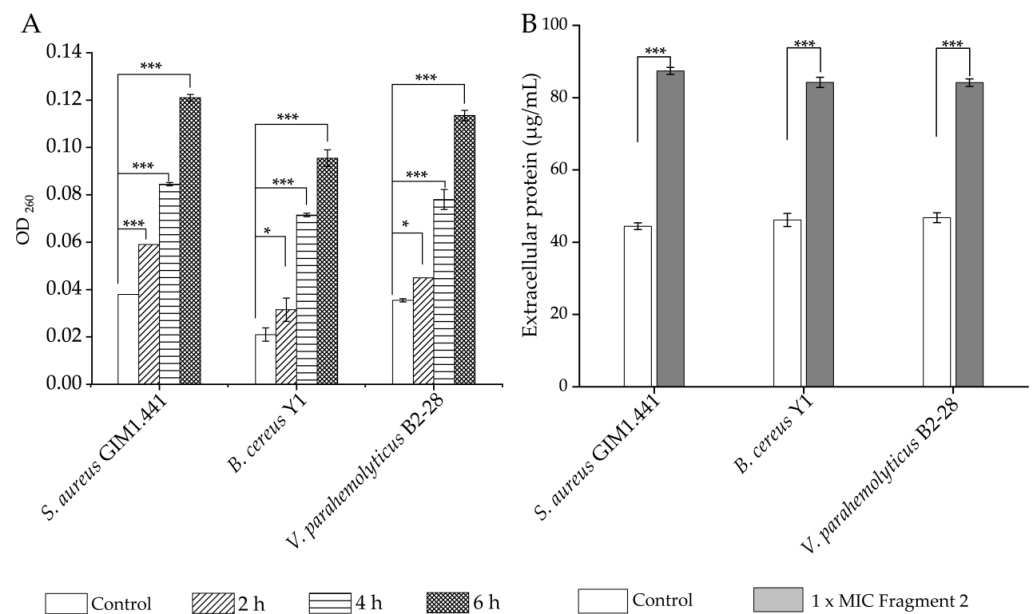


**Figure 6.** Effects of Fraction 2 of *A. villosum* Lour. on nucleotide acid and protein exudation of the target strains. (A,B): nucleotide acids and proteins, respectively. \*:  $p < 0.05$ ; and \*\*\*:  $p < 0.001$ .

As shown in Figure 6B, the number of extracellular proteins of *S. aureus* GIM1.441 was also significantly increased by 1.97-fold after being treated with Fraction 2 for 24 h ( $p < 0.001$ ). Likewise, the proteins were exuded by 1.82-fold and 1.80-fold from *B. cereus* Y1 and *V. parahemolyticus* B2-28, respectively, after the Fraction 2 treatment ( $p < 0.001$ ).

Bouyahya et al. [21] reported that the EO of *Origanum compactum* was involved in the changed membrane permeability and leakage of macromolecules. In this study, it can be concluded that the treatment with Fraction 2 of *A. villosum* Lour. results in the leakage of nucleotide acids and proteins from the Gram-positive and Gram-negative strains, consistent with the damaged bacterial cell structure observed with the SEM.

### 2.7. The Altered Metabolic Pathways in the Target Strains Treated with Fraction 2 of *A. villosum* Lour.

In order to obtain insights into the changes in gene expression at the whole-genome level, we determined the transcriptomes of *S. aureus* GIM1.441, *B. cereus* Y1, and *V. parahemolyticus* B2-28 treated with Fraction 2 (1 x MIC) for 6 h. The lists of the differential expressed genes (DEGs) in the three strains were deposited in the NCBI SRA database (<https://sub-mit.ncbi.nlm.nih.gov/subs/bioproject/>, accessed on 25 September 2023) under the accession number PRJNA1020669.

### 2.7.1. The Altered Metabolic Pathways in *S. aureus* GIM1.441 Treated with Fraction 2 of *A. villosum* Lour.

The DEGs in the treatment group accounted for 11.12% (291/2617) of the *S. aureus* GIM1.441 genes, as compared to the control group. Of these, 91 DEGs showed lower transcription levels (fold change (FC)  $\leq 0.5$ ), whereas 200 DEGs were up-regulated (FC  $\geq 2.0$ ). Eight metabolic pathways were significantly altered in *S. aureus* GIM1.441, including valine, leucine, and isoleucine biosynthesis; the biosynthesis of various other secondary metabolites; ascorbate and aldarate metabolism; C5-branched dibasic acid metabolism; alanine, aspartate, and glutamate metabolism; o-antigen nucleotide sugar biosynthesis; ribosome; and the biosynthesis of various antibiotics (Figure 7, Table S1).

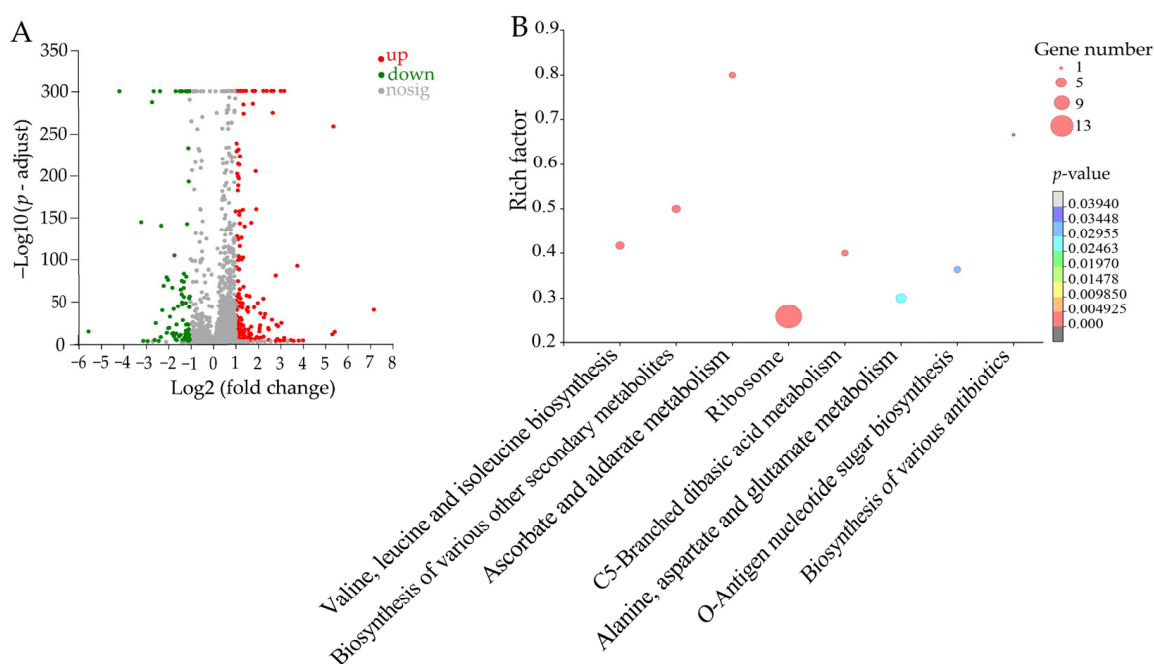


**Figure 7.** The eight significantly altered metabolic pathways in *S. aureus* GIM1.441 treated with Fraction 2 of *A. villosum* Lour. (A,B): Volcano plot of the DGEs and the changed metabolic pathways, respectively.

For example, the expression of three DEGs in valine, leucine, and isoleucine biosynthesis was significantly down-regulated (0.39- to 0.447-fold) at the transcriptional levels in *S. aureus* GIM1.441 after being treated with Fraction 2 of *A. villosum* Lour. ( $p < 0.05$ ). Of these, the ketol-acid reductoisomerase (*B4602\_RS10775*) was significantly repressed (0.447-fold) ( $p < 0.05$ ), which plays a crucial role in the biosynthesis pathway of branched-chain amino acids [22]. The 2-isopropylmalate synthase (*B4602\_RS10780*) was also significantly down-regulated (0.39-fold) ( $p < 0.05$ ), which catalyzes the first step of leucine biosynthesis [23]. The threonine ammonia-lyase IlvA (*B4602\_RS10800*) was significantly inhibited as well (0.394-fold) ( $p < 0.05$ ), which has been reported to resist the feedback inhibition of l-isoleucine [24].

In the C5 branched-chain binary acid metabolism, three DEGs were also significantly down-regulated (0.303- to 0.414-fold) ( $p < 0.05$ ). For example, the 3-isopropylmalate dehydrogenase (*B4602\_RS10785*) was significantly inhibited (0.379-fold) ( $p < 0.05$ ), which serves as the third specific enzyme for the synthesis of leucine in microorganisms and plants [25].

In alanine, aspartate, and glutamate metabolism, the expression of two DEGs was also significantly down-regulated (0.413- to 0.472-fold) in *S. aureus* GIM1.441 ( $p < 0.05$ ). For example, the adenylosuccinate synthase (*B4602\_RS00095*) was significantly inhibited (0.413-fold), which catalyzes the first committed step in the synthesis of adenosine [26]. Conversely, four DEGs were significantly up-regulated (2.014- to 2.141-fold), e.g., the

glutamate synthase large subunit (*B4602\_RS02195*) (2.141-fold). Li et al. reported that this enzyme may play a key role in the antimicrobial resistance in cocci through its involvement in folate metabolism or cell membrane integrity [27].

The ribosomes responsible for protein synthesis are one of the main antibiotic targets in bacterial cells [28,29]. The up-regulation of the ribosome metabolic pathway indicates accelerated cell division, which increases the likelihood of gene mutation. In this study, fifteen DEGs were significantly up-regulated (2.003- to 2.791-fold) in *S. aureus* GIM1.441 ( $p < 0.05$ ), e.g., 30S ribosomal protein S8 (*B4602\_RS11755*), 50S ribosomal protein L18 (*B4602\_RS11745*), and 50S ribosomal protein L5 (*B4602\_RS11765*).

Taken together, Fraction 2 of *A. villosum* Lour. altered the eight metabolic pathways in *S. aureus* GIM1.441, thereby likely inhibited the bacterial amino acid and secondary metabolite metabolisms, cell membrane biosynthesis, and resistance. The up-regulated expression of ribosome-related proteins may serve as a self-saving strategy for the bacterium to survive under the unfavorable circumstance elicited by the Fraction 2 treatment.

### 2.7.2. The Altered Metabolic Pathways in *B. cereus* Y1 Treated with Fraction 2 of *A. villosum* Lour.

The DEGs in the treatment group accounted for 44.45% (2363/5316) of the *B. cereus* Y1 genes. Of these, notably, 2173 DEGs were down-regulated ( $FC < 0.5$ ), whereas 190 DEGs were up-regulated ( $FC \geq 2.0$ ). Seven metabolic pathways were significantly altered in *B. cereus* Y1, including bacterial chemotaxis; nucleotide excision repair; histidine metabolism; mismatch repair; valine, leucine, and isoleucine degradation; the biosynthesis of siderophore group nonribosomal peptides; and o-antigen nucleotide sugar biosynthesis (Figure 8, Table S2).

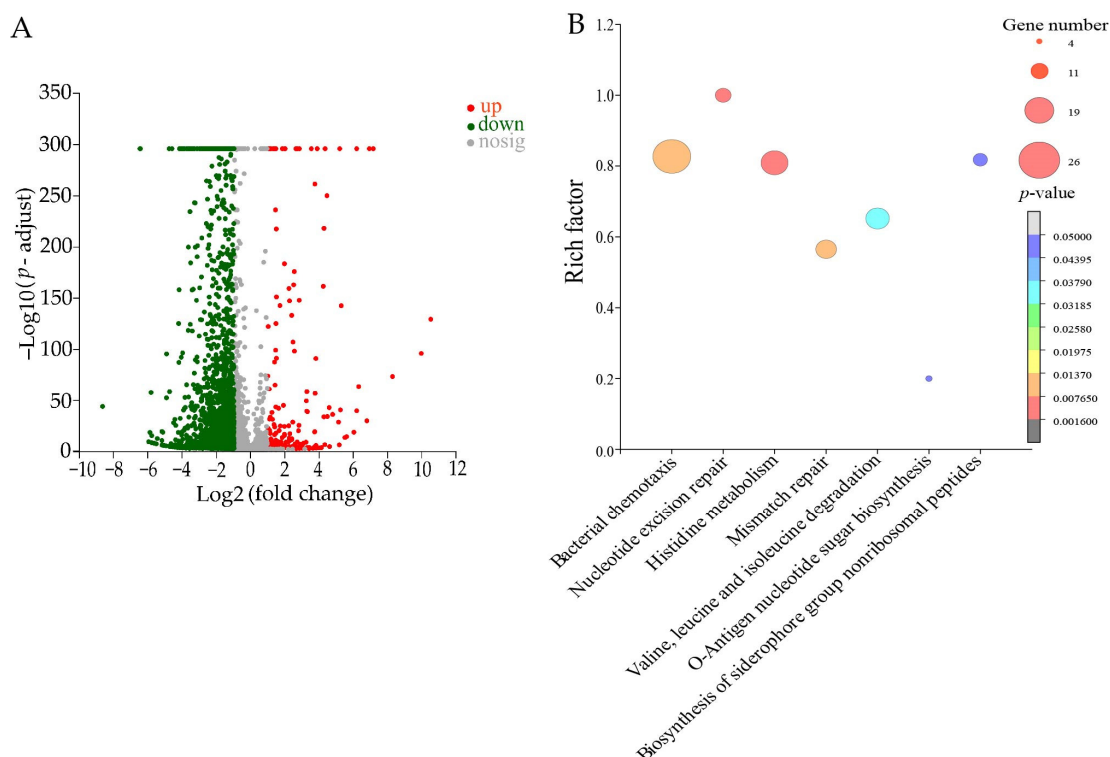


**Figure 8.** The significantly altered metabolic pathways in *B. cereus* Y1 treated with Fraction 2 of *A. villosum* Lour. (A,B): Volcano plot of the DGEs and the changed metabolic pathways, respectively.

For example, in the bacterial chemotaxis, the expression of 24 DEGs was significantly down-regulated (0.11- to 0.479-fold) at the transcriptional level in *B. cereus* Y1 after being treated with Fraction 2 ( $p < 0.05$ ), e.g., the methyl-accepting chemotaxis protein (MCP) (*EJ379\_25705*), chemotaxis signal transduction protein CheV (*EJ379\_08390*), flagellar mo-

tor protein MotB (*EJ379\_23055*), and glutamate O-methyltransferase CheR (*EJ379\_05155*). For instance, the MCP plays an important role in cell survival and biodegradation [30], and can also control the direction of flagella motors, promoting cell rolling and smooth swimming [31].

In nucleotide excision repair, ten DEGs were also significantly inhibited (0.18- to 0.431-fold) ( $p < 0.05$ ), e.g., the transcription-repair coupling factor (*EJ379\_00305*), DNA polymerase I (*EJ379\_23430*), NAD-dependent DNA ligase LigA (*EJ379\_01760*), and ATP-dependent helicase (*EJ379\_06255*). For example, LigA is crucial for DNA replication and repair in only bacteria and some viruses. LigAs have been reported to be attractive targets for antibacterial drugs [32].

In mismatch repair, the expression of 13 DEGs was significantly down-regulated (0.242- to 0.500-fold) in *B. cereus* Y1 ( $p < 0.05$ ). For example, the DNA mismatch repair endonuclease MutL (*EJ379\_19260*) was significantly repressed (0.332-fold). The MutL family of DNA mismatch repair proteins plays a key role in the cleavage and repair of mismatch errors during DNA replication [33].

In valine, leucine, and isoleucine degradation, 12 DEGs were significantly down-regulated (0.179- to 0.49-fold) ( $p < 0.05$ ); in o-antigen nucleotide sugar biosynthesis, 3 DEGs were significantly inhibited (0.073- to 0.018-fold) ( $p < 0.05$ ); and in the biosynthesis of the siderophore group nonribosomal peptides, 9 DEGs were significantly down-regulated as well (0.079- to 0.349-fold) ( $p < 0.05$ ).

Taken together, Fraction 2 of *A. villosum* Lour. altered the seven metabolic pathways in *B. cereus* Y1, thereby hindered the bacterial chemotaxis, flagellar movement, DNA replication and repair, and amino acid metabolisms, leading to its rupture and death.

### 2.7.3. The Altered Metabolic Pathways in *V. parahemolyticus* B2-28 Treated with Fraction 2 of *A. villosum* Lour.

The DEGs in the treatment group accounted for 19.30% (1081/5602) of the *V. parahemolyticus* B2-28 genes. Of these, 648 DEGs were down-regulated ( $FC \leq 0.5$ ), whereas 433 DEGs were up-regulated ( $FC \geq 2.0$ ). Remarkably, sixteen metabolic pathways were significantly altered in *V. parahemolyticus* B2-28, including glyoxylate and dicarboxylate metabolism; propanoate metabolism; lysine degradation; one carbon pool by folate; fatty acid degradation; methane metabolism; sulfur metabolism; one carbon pool by folate; ABC transporters; QS; arginine and proline metabolism; taurine and hypotaurine metabolism; purine metabolism; alpha-linolenic acid metabolism; non-alcoholic fatty liver disease; and butanoate metabolism (Figure 9, Table S3).

For example, in glyoxylate and dicarboxylate metabolism, the expression of eight DEGs was significantly inhibited (0.126-fold to 0.499-fold) in *V. parahemolyticus* B2-28 after being treated with Fraction 2 of *A. villosum* Lour., whereas two DEGs were significantly up-regulated (2.081- to 4.678-fold) ( $p < 0.05$ ). For instance, the multidrug transporter AcrB (*Vp\_B2\_28\_4316*) was highly repressed (0.126-fold), which is a component of the multidrug efflux pumps that play a key role in the process of bacterial resistance [34]. In contrast, the catalase (*Vp\_B2\_28\_0438*) was significantly up-regulated (2.081-fold), which has been reported to prevent cellular oxidative damage by decomposing hydrogen peroxide into water and oxygen [35].

In propanoate metabolism, the expression of nine DEGs was also significantly inhibited (0.199-fold to 0.432-fold) ( $p < 0.05$ ), e.g., the DNA mismatch repair protein MutT, histone acetyltransferase, and phosphoenolpyruvate protein phosphotransferase (PtsA). The latter was significantly down-regulated (0.264-fold), which is involved in the monosaccharide phosphotransferase system. Nebenzahl et al. [36] reported that the cell-wall-localized PtsA can function as an adhesin, and anti-PtsA antisera were shown to inhibit the adhesion of *S. pneumoniae* to cultured human lung adenocarcinoma cells A549.

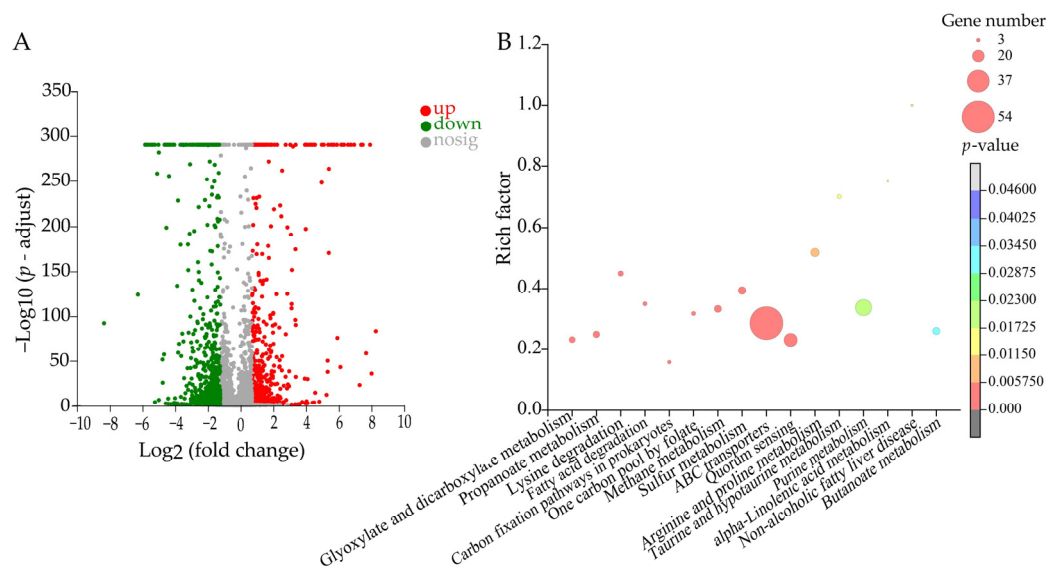


**Figure 9.** The significantly altered metabolic pathways in *V. parahemolyticus* B2-28 treated with Fraction 2 of *A. villosum* Lour. (A,B): Volcano plot of the DEGs and the changed metabolic pathways, respectively.

In lysine degradation, the expression of six DEGs was significantly inhibited (0.177-fold to 0.482-fold), whereas three DEGs were significantly up-regulated (2.086- to 3.719-fold) in *V. parahemolyticus* B2-28 ( $p < 0.05$ ). For instance, citrate (Si)-synthase (*Vp\_B2\_28\_3274*) was significantly down-regulated (0.453-fold), which catalyzes the initial reaction of the tricarboxylic acid cycle (TCA) [37]. In contrast, the heavy-metal-responsive transcriptional regulator (*Vp\_B2\_28\_3823*) was significantly up-regulated (2.086-fold), which plays a crucial role in metal uptake, isolation, oxidation, or reduction to lower toxicity by regulating the expression of detoxification-related genes [38].

In the ABC transporters, the expression of 43 DEGs was significantly inhibited (0.014-fold to 0.483-fold) and 12 DEGs were significantly up-regulated (2.073- to 27.425-fold) ( $p < 0.05$ ). For example, the oligopeptide ABC transporter ATP-binding protein OppF (*Vp\_B2\_28\_0132*) was significantly down-regulated (0.215-fold), which is essential for spirochete viability in vitro and during infection [39]. Moreover, the serine protease (*Vp\_B2\_28\_0735*) was also significantly inhibited (0.221-fold). The cell-membrane-binding serine protease plays an important role in maintaining cell homeostasis in pathobiology [40].

In the QS, the expression of 20 DEGs was significantly inhibited (0.116-fold to 0.495-fold) in *V. parahemolyticus* B2-28 ( $p < 0.05$ ). Many previous studies have indicated that the formation of QS and biofilm promotes the development of antibiotic resistance in microorganisms [41]. In this study, for example, the DEG encoding a ketol-acid reductoisomerase (KARI) (*Vp\_B2\_28\_4615*) was significantly down-regulated (0.434-fold), which has been reported to be a potential drug target against pathogenic bacteria [42].

In arginine and proline metabolism, the expression of 13 DEGs was significantly inhibited (0.071-fold to 0.284-fold) ( $p < 0.05$ ). In contrast, remarkably, the expression of endonuclease I (*Vp\_B2\_28\_2907*) was strongly enhanced (70.055-fold), suggesting that DNA breakage may have occurred in *V. parahaemolyticus* B2-28 after the Fraction 2 treatment.

In taurine and hypotaurine metabolism, the expression of four DEGs was significantly down-regulated (0.353- to 0.488-fold) in *V. parahaemolyticus* B2-28 ( $p < 0.05$ ). For instance, the RNA chaperone ProQ (*Vp\_B2\_28\_2494*) and tail-specific protease (*Vp\_B2\_28\_2495*) were repressed (0.353-fold and 0.42-fold). The former mediates sRNA-directed gene regulation in Gram-negative bacteria, while the latter is involved in tolerance to heat stress and virulence [43,44]. In addition, the DEG encoding a phage shock protein (Psp) G was greatly down-regulated (0.098-fold). The Psp stress response system can sense and respond to cell membrane damage [45].

Taken together, Fraction 2 of *A. villosum* Lour. significantly altered sixteen metabolic pathways in *V. parahemolyticus* B2-28, and thus hindered the amino acid metabolism, cell membrane biosynthesis, and substance transportation; and repressed the intercellular communication, stress regulation, and virulence, leading to cellular oxidative damage, DNA breakage, and cell death.

Additionally, to validate the transcriptome data, we performed real-time reverse transcription quantitative PCR (RT-qPCR) analysis on fifteen representative DEGs, and the obtained results were generally consistent with the transcriptome data (Tables S4 and S5).

#### 2.7.4. Antibacterial Modes of Fraction 2 of *A. villosum* Lour.

As shown in Table S6, Fraction 2 of *A. villosum* Lour. displayed different antibacterial modes against the Gram-positive and Gram-negative bacteria and hindered a series of metabolic pathways, leading to varying levels of cell damage and even death. On the other hand, the same metabolic pathways, such as o-antigen nucleotide sugar biosynthesis and valine, leucine, and isoleucine metabolisms, were all inhibited in the Gram-positive bacteria *S. aureus* GIM1.441 and *B. cereus* Y1 by Fraction 2. Additionally, some metabolic pathways were only hindered in the Gram-negative bacterium *parahemolyticus* B2-28 by Fraction 2, such as the repressed substance transporting, intercellular communication, stress regulation, and virulence.

Overall, the results of this study demonstrate that Fraction 2 of *A. villosum* Lour. exerts the strongest inhibitory efficacy on the Gram-negative bacterium *V. parahemolyticus* B2-28, followed by the Gram-positive bacteria *B. cereus* Y1 and *S. aureus* GIM1.441 through multiple antibacterial modes.

#### 2.8. Identification of Potential Antibacterial Compounds in Fraction 2 of *A. villosum* Lour.

Based on the above results, we wondered what compounds functioned in Fraction 2 of *A. villosum* Lour. Therefore, the antibacterial components of Fraction 2 were further identified using the ultra-HPLC and mass spectrometry (UHPLC-MS) technique. As shown in Table 3, eighty-nine compounds were identified. The most abundant compound in Fraction 2 was 4-hydroxyphenylacetylglutamic acid (30.89%), followed by lubiprostone (11.86%), miltirone (10.68%), oleic acid (10.58%), and oxymorphone (5.69%). The other compounds (4.81–0.10%), such as alkaloids, flavonoids, phenols, and coumarins, were also identified (Table 3).

**Table 3.** Potential antibacterial compounds identified in Fraction 2 of *A. villosum* Lour. by the UHPLC-MS analysis.

Identified Compound	Rt (min)	Compound Nature	Formula	Exact Mass	Fraction Area (%)
4-Hydroxyphenylacetylglutamic acid	12.99	Glutamate and derivatives	C <sub>13</sub> H <sub>15</sub> NO <sub>6</sub>	281.09	30.89%
Lubiprostone	12.75	Fatty acyls	C <sub>20</sub> H <sub>32</sub> F <sub>2</sub> O <sub>5</sub>	390.22	11.86%
Miltirone	12.98	Diterpenoids	C <sub>19</sub> H <sub>22</sub> O <sub>2</sub>	282.16	10.68%
Oleic acid	13.03	Fatty acyls	C <sub>18</sub> H <sub>34</sub> O <sub>2</sub>	282.26	10.58%
Oxymorphone	11.18	Morphinane and derivatives	C <sub>17</sub> H <sub>19</sub> NO <sub>4</sub>	301.13	5.69%
Piperlonguminine	10.57	Alkaloids	C <sub>16</sub> H <sub>19</sub> NO <sub>3</sub>	273.14	4.81%
Adenosine	2.58	Amino acid and derivatives	C <sub>10</sub> H <sub>13</sub> N <sub>5</sub> O <sub>4</sub>	267.1	3.74%
Nandrolone	10.58	Steroids and steroid derivatives	C <sub>18</sub> H <sub>26</sub> O <sub>2</sub>	274.19	2.89%

Table 3. Cont.

Identified Compound	Rt (min)	Compound Nature	Formula	Exact Mass	Fraction Area (%)
Palmitic acid	12.92	Lipids	C <sub>16</sub> H <sub>32</sub> O <sub>2</sub>	256.24	2.64%
Sarracine	13.14	Alkaloids	C <sub>18</sub> H <sub>27</sub> NO <sub>5</sub>	337.19	2.27%
Glucose 1-phosphate	13.00	Organo-oxygen compounds	C <sub>6</sub> H <sub>13</sub> O <sub>9</sub> P	260.03	2.23%
Artemisinin	13.02	Sesquiterpenoids	C <sub>15</sub> H <sub>22</sub> O <sub>5</sub>	282.15	1.83%
Erucic acid	13.28	Fatty acyls	C <sub>22</sub> H <sub>42</sub> O <sub>2</sub>	338.32	0.93%
2-Phenylacetamide	2.52	Benzene and substituted derivatives	C <sub>8</sub> H <sub>9</sub> NO	135.07	0.92%
Crotonoside	2.40	Alkaloids	C <sub>10</sub> H <sub>13</sub> N <sub>5</sub> O <sub>5</sub>	283.09	0.76%
22-Dehydroclerosterol	12.59	Steroids	C <sub>29</sub> H <sub>46</sub> O	410.35	0.72%
Guanine	2.63	Nucleotide and derivatives	C <sub>5</sub> H <sub>5</sub> N <sub>5</sub> O	151.05	0.64%
Wighteone	13.01	Flavonoids	C <sub>20</sub> H <sub>18</sub> O <sub>5</sub>	338.12	0.52%
4-Hydroxybenzaldehyde	1.91	Phenols	C <sub>7</sub> H <sub>6</sub> O <sub>2</sub>	122.04	0.47%
Octadecanamide	13.02	Fatty acyls	C <sub>18</sub> H <sub>37</sub> NO	283.29	0.47%
8-Geranyloxypsoralen	13.29	Coumarins	C <sub>21</sub> H <sub>22</sub> O <sub>4</sub>	338.15	0.45%
Kirenol	13.03	Diterpenoids	C <sub>20</sub> H <sub>34</sub> O <sub>4</sub>	338.25	0.34%
7-(4-Hydroxyphenyl)-1-phenyl-4-hepten-3-one	12.53	Phenols	C <sub>19</sub> H <sub>20</sub> O <sub>2</sub>	280.15	0.32%
Glycerophosphocholine	12.87	Cholines	C <sub>8</sub> H <sub>20</sub> NO <sub>6</sub> P	257.22	0.30%
Supinine	12.99	Alkaloids	C <sub>15</sub> H <sub>25</sub> NO <sub>4</sub>	283.18	0.27%
Octyl gallate	12.97	Phenols	C <sub>15</sub> H <sub>22</sub> O <sub>5</sub>	282.15	0.22%
Inosine	2.60	Nucleotide and derivatives	C <sub>10</sub> H <sub>12</sub> N <sub>4</sub> O <sub>5</sub>	268.08	0.21%
Moracin C	13.99	Phenols	C <sub>19</sub> H <sub>18</sub> O <sub>4</sub>	310.12	0.20%
AICA-riboside	13.28	Imidazole ribonucleosides and ribonucleotides	C <sub>9</sub> H <sub>15</sub> N <sub>4</sub> O <sub>8</sub> P	338.06	0.19%
Glucose 1-phosphate	13.03	Organo-oxygen compounds	C <sub>6</sub> H <sub>13</sub> O <sub>9</sub> P	260.03	0.14%
Kirenol	13.16	Diterpenoids	C <sub>20</sub> H <sub>34</sub> O <sub>4</sub>	338.25	0.12%
Isoquercitrin	6.06	Flavonoids	C <sub>21</sub> H <sub>20</sub> O <sub>12</sub>	464.1	0.10%
Oleamide	12.54	Fatty acyls	C <sub>18</sub> H <sub>35</sub> NO	281.27	0.10%
DL-Tyrosine	1.90	Monophenols amino acids	C <sub>9</sub> H <sub>11</sub> NO <sub>3</sub>	181.07	0.08%
L-Pipecolic acid	0.69	Amino acid and derivatives	C <sub>6</sub> H <sub>11</sub> NO <sub>2</sub>	129.08	0.08%
Stearic acid	13.02	Fatty acyls	C <sub>18</sub> H <sub>36</sub> O <sub>2</sub>	284.27	0.07%
Panaxynol	12.57	Miscellaneous	C <sub>17</sub> H <sub>24</sub> O	244.18	0.06%
Xanthosine	2.61	Nucleotide and derivatives	C <sub>10</sub> H <sub>12</sub> N <sub>4</sub> O <sub>6</sub>	284.08	0.05%
N1-Methyl-4-pyridone-3-carboxamide	2.66	Pyridines and derivatives	C <sub>7</sub> H <sub>8</sub> N <sub>2</sub> O <sub>2</sub>	152.06	0.05%
2-(2-Hydroxy-2-propyl)-5-methyl-5-vinyltetrahydrofuran	5.47	Monoterpenoids	C <sub>10</sub> H <sub>18</sub> O <sub>2</sub>	170.13	0.05%
α-Isopropylmalate	10.79	Nucleotide and derivatives	C <sub>7</sub> H <sub>12</sub> O <sub>5</sub>	176.07	0.04%
Isoquercitrin	6.22	Flavonoids	C <sub>21</sub> H <sub>20</sub> O <sub>12</sub>	464.1	0.04%
Bergamotone	13.03	Coumarins	C <sub>21</sub> H <sub>22</sub> O <sub>4</sub>	338.15	0.04%
Seneciphylline	9.06	Alkaloids	C <sub>18</sub> H <sub>23</sub> NO <sub>5</sub>	333.16	0.03%

Table 3. Cont.

Identified Compound	Rt (min)	Compound Nature	Formula	Exact Mass	Fraction Area (%)
Cianidanol	4.50	Flavonoids	C <sub>15</sub> H <sub>14</sub> O <sub>6</sub>	290.08	0.03%
3,4,5-Trimethoxycinnamyl alcohol	10.40	Phenylpropanoids	C <sub>12</sub> H <sub>16</sub> O <sub>4</sub>	224.1	0.03%
Procyanidin B2	4.78	Flavonoids	C <sub>30</sub> H <sub>26</sub> O <sub>12</sub>	578.14	0.03%
(Z)-Aconitic acid	1.46	Organic acids and derivatives	C <sub>6</sub> H <sub>6</sub> O <sub>6</sub>	174.02	0.03%
Astragalin	6.52	Flavonoids	C <sub>21</sub> H <sub>20</sub> O <sub>11</sub>	448.1	0.03%
Kazinol A	13.26	Phenols	C <sub>25</sub> H <sub>30</sub> O <sub>4</sub>	394.21	0.02%
Epifriedelanol	12.29	Terpenoids	C <sub>30</sub> H <sub>52</sub> O	428.4	0.02%
Stigmasterol	13.12	Steroids	C <sub>29</sub> H <sub>48</sub> O	412.37	0.02%
4-Propylphenol	10.56	Benzene and substituted derivatives	C <sub>9</sub> H <sub>12</sub> O	136.09	0.02%
Kaempferol-3-O-glucorhamnoside	6.29	Flavonoids	C <sub>27</sub> H <sub>30</sub> O <sub>15</sub>	594.16	0.02%
Geranyl acetate	9.58	Monoterpenoids	C <sub>12</sub> H <sub>20</sub> O <sub>2</sub>	196.15	0.01%
Tilioside	7.92	Flavonoids	C <sub>30</sub> H <sub>26</sub> O <sub>13</sub>	594.14	0.01%
3,4-Dihydrocoumarin	6.68	Coumarins	C <sub>9</sub> H <sub>8</sub> O <sub>2</sub>	148.05	0.01%
20-HETE	13.28	Fatty acyls	C <sub>20</sub> H <sub>32</sub> O <sub>3</sub>	320.24	0.01%
Herniarin	7.69	Coumarins	C <sub>10</sub> H <sub>8</sub> O <sub>3</sub>	176.05	0.01%
Fingolimod hydrochloride	13.11	Sphingosine analogues	C <sub>19</sub> H <sub>34</sub> C <sub>1</sub> NO <sub>2</sub>	343.93	0.01%
4-Hydroxybenzoic acid	1.08	Phenols	C <sub>7</sub> H <sub>6</sub> O <sub>3</sub>	138.03	0.01%
D-Glucuronic acid lactone	4.22	Ketones	C <sub>6</sub> H <sub>8</sub> O <sub>6</sub>	176.03	0.01%
Tricetin	8.05	Flavonoids	C <sub>15</sub> H <sub>10</sub> O <sub>7</sub>	302.04	0.01%
Benzocaine	3.05	Benzene and substituted derivatives	C <sub>9</sub> H <sub>11</sub> NO <sub>2</sub>	165.08	0.01%
Taxiphyllin	13.33	Phenols	C <sub>14</sub> H <sub>17</sub> NO <sub>7</sub>	311.1	0.01%
Thymol	10.86	Phenols	C <sub>10</sub> H <sub>14</sub> O	150.1	0.01%
5-Aminovaleric acid	1.11	Amino acid and derivatives	C <sub>5</sub> H <sub>11</sub> NO <sub>2</sub>	117.08	0.01%
3,5,7-Trimethoxyflavone	10.8	Flavonoids	C <sub>18</sub> H <sub>16</sub> O <sub>5</sub>	312.1	0.01%
N-Methyl-4-pyridone-3-carboxamide	2.63	Pyridines and derivatives	C <sub>7</sub> H <sub>8</sub> N <sub>2</sub> O <sub>2</sub>	152.06	0.01%
9,10-DiHOME	13.3	Linoleic acid diol derivative	C <sub>18</sub> H <sub>34</sub> O <sub>4</sub>	314.25	0.01%
Physalin O	12.39	Steroids and derivatives	C <sub>28</sub> H <sub>32</sub> O <sub>10</sub>	528.2	0.01%
Azelaic acid	6.81	Organic acids	C <sub>9</sub> H <sub>16</sub> O <sub>4</sub>	188.1	0.01%
3-Indolebutyric acid	9.00	Alkaloids	C <sub>12</sub> H <sub>13</sub> NO <sub>2</sub>	203.09	0.01%
Rutin	5.85	Flavonoids	C <sub>27</sub> H <sub>30</sub> O <sub>16</sub>	610.15	0.01%
Niazirin	12.54	Saccharides	C <sub>14</sub> H <sub>17</sub> NO <sub>5</sub>	279.11	0.01%
1-Octacosanol	13.20	Fatty alcohol	C <sub>28</sub> H <sub>58</sub> O	410.45	0.01%
Limonexic acid	12.55	Triterpenoids	C <sub>26</sub> H <sub>30</sub> O <sub>10</sub>	502.18	0.01%
Taraxasterone	13.85	Triterpenoids	C <sub>30</sub> H <sub>48</sub> O	424.37	0.01%
Mitraphylline	13.02	Alkaloids	C <sub>21</sub> H <sub>24</sub> N <sub>2</sub> O <sub>4</sub>	368.17	0.01%
DL- $\alpha$ -Tocopherol acetate	13.37	Vitamin E derivatives	C <sub>31</sub> H <sub>52</sub> O <sub>3</sub>	472.39	0.01%
Trans-Cinnamaldehyde	6.34	Phenylpropanoids	C <sub>9</sub> H <sub>8</sub> O	132.06	0.01%
Caffeoyl alcohol	10.09	Phenols	C <sub>9</sub> H <sub>10</sub> O <sub>3</sub>	166.06	0.01%
Calycosin	9.10	Flavonoids	C <sub>16</sub> H <sub>12</sub> O <sub>5</sub>	284.07	0.01%
Biochanin A	11.38	Flavonoids	C <sub>16</sub> H <sub>12</sub> O <sub>5</sub>	284.07	0.01%
Nicotiflorin	12.34	Flavonoids	C <sub>27</sub> H <sub>30</sub> O <sub>15</sub>	594.16	0.01%
Tilioside	8.17	Flavonoids	C <sub>30</sub> H <sub>26</sub> O <sub>13</sub>	594.14	0.01%
1-Isomangostin	13.16	Xanthenes	C <sub>24</sub> H <sub>26</sub> O <sub>6</sub>	410.17	0.01%
Sterebin F	13.03	Terpenoids	C <sub>20</sub> H <sub>34</sub> O <sub>4</sub>	338.25	0.01%
6,8-Diprenylnaringenin	12.62	Flavonoids	C <sub>25</sub> H <sub>28</sub> O <sub>5</sub>	408.19	0.01%

The 4-hydroxyphenylacetylglutamic identified in this study is an acetyl compound of glutamate. It has been reported that this compound can pass through the blood–brain barrier, improve nerve cell metabolism, maintain nervous stress, and reduce blood ammonia [46]. The lubiprostone identified in this study can safely and effectively treat chronic idiopathic constipation and irritable bowel syndrome with constipation [47]. Terpenoids, such as the miltirone identified in this study, have enormous inhibitory potential against microorganisms through different mechanisms such as membrane disruption, anti-QS, and protein and ATP synthesis inhibition [48]. The 8-Geranyloxypsoralen, bergamotone, and 3,4-Dihydrocoumarin identified in this study are coumarins, with pharmacological activities such as antibacterial, anti-inflammatory, and anti-cancer [49]. The piperlonguminine identified in this study is a compound of the alkaloid class that has been proved to have anti-inflammatory activity [50]. The isoquercitrin identified in this study has a variety of chemical protection effects in vitro and in vivo against oxidative stress, cancer, cardiovascular disease, diabetes, and allergic reaction [51].

Taken together, these results have revealed potential antibacterial compounds in Fraction 2 of *A. villosum* Lour., a promising antibacterial source of natural products.

The major limitation of this study was that the top compounds identified in Fraction 2 were not available commercially, therefore, the antibacterial activity of each compound could not be analyzed. It would be interesting to continue with the proposed analysis through a chemical synthesis method to obtain single compounds in future research.

### 3. Materials and Methods

#### 3.1. Bacterial Strains and Culture Conditions

The bacterial strains and media used in this study are shown in Table S7. The incubation conditions of the bacterial strains were the same as those described in our recent reports [11–14].

#### 3.2. Extraction of Bacteriostatic Substances from *A. villosum* Lour.

The fresh fruit samples were purchased from the production base of *A. villosum* Lour. in Yangchun City (22°41′01″ N, 111°16′27″ E), Guangdong Province, China (Figure S2). The fruit is oval, purplish red when ripe, and brown after dry, with a unique and rich aroma. The antibacterial components in the samples were extracted using the M–CE method, as reported in our recent studies [11–14]. Briefly, the fresh samples were washed with water, cut into small pieces of about 1/4 size, and pre-frozen at  $-80^{\circ}\text{C}$  for 8 h. Thereafter, the samples were further freeze-dried, crushed, and extracted with the methanol–chloroform (2:1, *v/v*, analytical grade, Merck KGaA, Darmstadt, Germany) at a solid-to-liquid ratio of 1:10 (*m/v*) for 5 h. A certain amount of  $\text{H}_2\text{O}$  (analytical grade) was added, sonicated, and filtered, and then the MPE and CPE were separated using the same equipment and parameters described in our recent reports [11–14].

#### 3.3. Antibacterial Activity Assay

The sensitivity of the bacterial strains to the MPE and CPE from *A. villosum* Lour. was measured according to the standard method approved by the Clinical and Laboratory Standards Institute, Malvern, PA, USA (CLSI, M100-S23, 2018). The MICs of the extracts from *A. villosum* Lour. were determined against the target strains. The definition of antibacterial activity and MICs were described in our recent reports [11–14].

#### 3.4. Prep-HPLC Analysis

The MPE of *A. villosum* Lour. was isolated using a Waters 2707 autosampler (Waters, Milford, MA, USA) linked with a UPLC Sunfire  $\text{C}_{18}$  column (Waters, Milford, MA, USA). The parameters of the Prep-HPLC analysis were the same as those described in our recent reports [11–14].

### 3.5. UHPLC-MS Analysis.

The UHPLC-MS analysis was carried out by Shanghai Hoogen Biotech, Shanghai, China, using the EXIONLC system (Sciex, Framingham, MA, USA). The running parameters of the UHPLC-MS were the same as those described in our recent reports [11–14].

### 3.6. Growth Curve Assay

The 1 × MIC and 1/2 × MIC of Fraction 2 of *A. villosum* Lour. were individually added into the bacterial cell culture of the target strains at the mid-logarithmic growth phase (mid-LGP) and then incubated at 37 °C for 24 h. The growth curves of the target strains were determined using the automatic growth curve analyzer (Synergy, BioTek Instruments, Winooski, VT, USA).

### 3.7. SEM Assay

Fraction 2 (1 × MIC) of *A. villosum* Lour. was added into the bacterial cell culture of the target strains and then incubated at 37 °C for 2 h, 4 h, and 6 h, respectively. Bacterial cells were then harvested by centrifugation at 4000 rpm at 4 °C for 10 min, then fixed with 2.50% glutaraldehyde (Shanghai Sangon Biological Engineering Technology and Service Co., Ltd., Shanghai, China) at 4 °C for 12 h, and dehydrated in the gradient ethanol (30%, 50%, 80%, 90%, and 100%) (Sangon, Shanghai, China) for 15 min, respectively. The samples were observed using the SEM (Hitachi, SU5000, Tokyo, Japan, 5.0 kV, x30,000) [11–14].

### 3.8. The CSH, CMF, and CMP Assays

The CSH of the target strains was determined according to the method of Cui et al. [52]. Briefly, the target strains at the mid-LGP were treated with Fraction 2 of *A. villosum* Lour for 2 h, 4 h, and 6 h, respectively. A total of 1 mL of hexadecane (National Pharmaceutical Group Corporation Co., Ltd., Shanghai, China) was added to an equal volume of the treated bacterial suspension, mixed for 1 min, and set at 37 °C for 30 min. Thereafter, the absorbance values of the mixture were measured at 600 nm. The CMF of the target strains was determined using the DPH (Sangon, Shanghai, China) as a probe, according to the method described in our recent reports [11–14]. The CMP of the target strains was measured using the OPNG (Beijing Solarbio Science & Technology Co., Ltd., Beijing, China) as a probe [11–14].

### 3.9. Bacterial Nucleotide Acid and Protein Exudation Assays

The nucleotide acid exudation of the target strains was measured according to the method of Lin et al. [53], with minor modifications. Briefly, the bacterial cell culture at the mid-LGP was treated with Fraction 2 (1 × MIC) of *A. villosum* Lour for 2 h, 4 h, and 6 h, respectively. The bacterial cell suspension was centrifuged at 4 °C at 3500 rpm for 5 min. Thereafter, the absorbance values of the supernatant were measured at 260 nm.

The bacterial protein exudation was determined according to the method of Atta et al. [54]. Briefly, Fraction 2 (1 × MIC) of *A. villosum* Lour was added into the bacterial cell culture at the mid-LGP and then incubated at a stationary condition at 37 °C for 24 h. The extracellular protein concentrations were determined using the Bradford method protein concentration determination kit (Sangong, Shanghai, China) according to the manufacturer's instructions.

### 3.10. Illumina RNA Sequencing

The bacterial cell culture at the mid-LGP of the target strains was individually treated with Fraction 2 (1 × MIC) of *A. villosum* Lour for 6 h. The total RNA of the harvested bacterial cells was extracted, purified, and analyzed, as described in our recent reports [11–14]. Three independently prepared RNA samples were used for each Illumina RNA-sequencing analysis, which was conducted by Shanghai Majorbio Bio-pharm Technology Co., Ltd. (Shanghai, China) using Illumina HiSeq 2500 platform (Illumina, Santiago, CA, USA) [11–14].

### 3.11. RT-qPCR Assay

The RT-qPCR assay was performed using the same kits and instrument outlined in the method described previously [55]. The oligonucleotide primers (Table S5) were designed using Premier 5.0 software (<https://www.premierbiosoft.com> (accessed on 28 September 2023)), and synthesized by Sangon, Shanghai, China.

### 3.12. Data Analysis

The DEGs were defined, and the altered metabolic pathways were analyzed by referring to the methods described in our recent studies [11–14]. All tests were conducted in triplicate, and the experimental data were analyzed using the SPSS version 17.0 software (SPSS Inc., Armonk, NY, USA).

## 4. Conclusions

In this study, we first investigated the antibacterial ingredients and modes of the MPE from the fruit of the pharmacophagous plant *A. villosum* Lour. The antibacterial rate of the MPE was 63.60%, targeting 22 species of common pathogenic bacteria. The MPE inhibited 2 species of Gram-positive bacteria, *S. aureus* and *B. cereus*; and 12 species of Gram-negative bacteria, *A. hydrophila*, *P. aeruginosa*, *S. dysenteriae*, *S. flexneri*, *S. sonnei*, *S. enterica* subsp. *enterica* (ex Kauffmann and Edwards), *V. alginolyticus*, *V. cholerae*, *V. harveyi*, *V. metschnikovi*, *V. mimicus*, and *V. parahaemolyticus*. The CPE showed an inhibition rate of 54.55% and inhibited one species of Gram-positive bacteria and 11 species of Gram-negative bacteria.

The MPE was further purified by Prep-HPLC, and three different constituents (Fractions 1–3) were obtained. Of these, the Fraction 2 treatment significantly increased the CMF and CMP, reduced the CSH, and damaged the integrity of the cell structure, leading to the leakage of the cellular macromolecules of Gram-positive *S. aureus* GIM1.441 and *B. cereus* Y1 and Gram-negative *V. parahemolyticus* B2-28 ( $p < 0.05$ ). Eighty-nine compounds in Fraction 2 were identified by the UHPLC-MS analysis, among which 4-hydroxyphenylacetylglutamic acid accounted for the highest 30.89%, followed by lubiprostone (11.86%), miltirone (10.68%), and oleic acid (10.58%).

Comparative transcriptomics analysis revealed a series of significantly altered metabolic pathways in the representative Gram-positive and Gram-negative target strains treated with Fraction 2 ( $p < 0.05$ ), indicating multiple antibacterial modes, e.g., hindering the amino acid metabolism and cell membrane biosynthesis, repressing the stress regulation and virulence, and leading to DNA breakage and cell death. Fraction 2 exerted the strongest inhibiting efficiency on Gram-negative *V. parahemolyticus* B2-28, followed by Gram-positive *B. cereus* Y1 and *S. aureus* GIM1.441.

Overall, this study first demonstrates the antibacterial activity of the MPE from the fruit of *A. villosum* Lour. and has provided data for its application in the medicinal and food preservative industries against common pathogens.

**Supplementary Materials:** The following supporting information can be downloaded at: <https://www.mdpi.com/article/10.3390/plants13060834/s1>, Table S1: The major altered metabolic pathways in *S. aureus* GIM1.441 treated with Fraction 2 of *A. villosum* Lour.; Table S2: The major altered metabolic pathways in *B. cereus* Y1 treated with Fraction 2 of *A. villosum* Lour.; Table S3: The major altered metabolic pathways in *V. parahemolyticus* B2-28 treated with Fraction 2 of *A. villosum* Lour.; Table S4: Comparison of the major altered metabolic pathways in the three target strains treated with Fraction 2 of *A. villosum* Lour.; Table S5: The oligonucleotide primers designed and used in the RT-qPCR assay; Table S6: The relative expression of the representative DEGs by the RT-qPCR assay; Table S7: The bacterial strains and media used in this study; Figure S1: Growth curves of the target strains treated with Fraction 2 of *A. villosum* Lour. (A–C): *S. aureus* GIM1.441, *B. cereus* Y1, and *V. parahemolyticus* B2-28, respectively. The strains were incubated in the TSB medium at 37 °C; Figure S2. The plant of *A. villosum* Lour. (A–C): the different plant growth periods.

**Author Contributions:** K.Z.: major experiments, data curation, and writing—original draft; F.C.: writing—original draft; Y.Z.: equipment support and help with the Prep-HPLC analysis; H.W.: supervision and writing—review and editing; L.C.: funding acquisition, conceptualization, and writing—review and editing. All authors have read and agreed to the published version of the manuscript.

**Funding:** This work was supported by the Science and Technology Commission of Shanghai Municipal, grant 17050502200.

**Data Availability Statement:** Data are contained within the article and Supplementary Materials. The complete lists of the DEGs in the three target strains are available in the NCBI SRA database (<https://sub-mit.ncbi.nlm.nih.gov/subs/bioproject/>, accessed on 25 September 2023) under the accession number PRJNA1020669.

**Acknowledgments:** The authors are grateful to Lianzhi Yang at Shanghai Ocean University for his help with the experiments.

**Conflicts of Interest:** The authors declare no conflicts of interest.

## References

1. Chow, F.W. Genomics: Infectious disease and host-pathogen interaction. *Int. J. Mol. Sci.* **2023**, *24*, 1748. [CrossRef] [PubMed]
2. Chapman, B.; Gunter, C. Local food systems food safety concerns. *Microbiol. Spectr.* **2018**, *6*, 1–9. [CrossRef] [PubMed]
3. Chang, R.Y.K.; Nang, S.C.; Chan, H.K.; Li, J. Novel antimicrobial agents for combating antibiotic-resistant bacteria. *Adv. Drug Deliv. Rev.* **2022**, *187*, 114378. [CrossRef] [PubMed]
4. Li, C.; Cui, Z.; Deng, S.; Chen, P.; Li, X.; Yang, H. The potential of plant extracts in cell therapy. *Stem Cell Res. Ther.* **2022**, *13*, 472. [CrossRef] [PubMed]
5. Cai, R.; Yue, X.; Wang, Y.; Yang, Y.; Sun, D.; Li, H.; Chen, L. Chemistry and bioactivity of plants from the genus *Amomum*. *J. Ethnopharmacol.* **2021**, *281*, 114563. [CrossRef] [PubMed]
6. Ma, M.; Lu, B. The complete chloroplast genome sequence of *Amomum villosum* Lour. *Mitochondrial DNA Part B—Resour.* **2020**, *5*, 1042–1043. [CrossRef] [PubMed]
7. Chen, S.; Chen, J.; Xu, Y.; Wang, X.; Li, J. Elsholtzia: A genus with antibacterial, antiviral, and anti-inflammatory advantages. *J. Ethnopharmacol.* **2022**, *297*, 115549. [CrossRef]
8. Yin, H.; Dan, W.J.; Fan, B.Y.; Guo, C.; Wu, K.; Li, D.; Xian, K.F.; Pescitelli, G.; Gao, J.M. Anti-inflammatory and  $\alpha$ -glucosidase inhibitory activities of labdane and norlabdane diterpenoids from the rhizomes of *Amomum villosum*. *J. Nat. Prod.* **2019**, *82*, 2963–2971. [CrossRef]
9. Luo, D.; Zeng, J.; Guan, J.; Xu, Y.; Jia, R.B.; Chen, J.; Jiang, G.; Zhou, C. Dietary supplement of *Amomum villosum* Lour. polysaccharide attenuates ulcerative colitis in balb/c mice. *Foods* **2022**, *11*, 3737. [CrossRef]
10. Tang, C.; Chen, J.; Zhang, L.; Zhang, R.; Zhang, S.; Ye, S.; Zhao, Z.; Yang, D. Exploring the antibacterial mechanism of essential oils by membrane permeability, apoptosis and biofilm formation combination with proteomics analysis against methicillin-resistant *Staphylococcus aureus*. *Int. J. Med. Microbiol.* **2020**, *10*, 151435. [CrossRef]
11. Tang, Y.; Yu, P.; Chen, L. Identification of antibacterial components and modes in the methanol-phase extract from a herbal plant *Potentilla kleiniana* Wight Et Arn. *Foods* **2023**, *12*, 1640. [CrossRef] [PubMed]
12. Liu, Y.; Tang, Y.; Ren, S.; Chen, L. Antibacterial components and modes of the methanol-phase extract from *Commelina communis* Linn. *Plants* **2023**, *12*, 890. [CrossRef] [PubMed]
13. Fu, J.; Wang, Y.; Sun, M.; Xu, Y.; Chen, L. Antibacterial activity and components of the methanol-phase extract from rhizomes of pharmacophagous plant *Alpinia officinarum* hance. *Molecules* **2022**, *27*, 4308. [CrossRef] [PubMed]
14. Liu, Y.; Yang, L.; Liu, P.; Jin, Y.; Qin, S.; Chen, L. Identification of antibacterial components in the methanol-phase extract from edible herbaceous plant *Rumex madaio* makino and their antibacterial action modes. *Molecules* **2022**, *27*, 660. [CrossRef] [PubMed]
15. Ahmad-Mansour; Loubet, P.; Pouget, C.; Dunyach-Remy, C.; Sotto, A.; Lavigne, J.P.; Molle, V. *Staphylococcus aureus* toxins: An update on their pathogenic properties and potential treatments. *Toxins* **2021**, *13*, 677. [CrossRef] [PubMed]
16. Prince, C.; Kovac, J. Regulation of enterotoxins associated with *Bacillus cereus* sensu lato toxicoinfection. *Appl. Environ. Microbiol.* **2022**, *88*, e0040522. [CrossRef] [PubMed]
17. Liu, W.; Ou, P.; Tian, F.; Liao, J.; Ma, Y.; Wang, J.; Jin, X. Anti-*Vibrio parahaemolyticus* compounds from *Streptomyces parvus* based on Pan-genome and subtractive proteomics. *Front. Microbiol.* **2023**, *14*, 1218176. [CrossRef] [PubMed]
18. Vij, R.; Danchik, C.; Crawford, C.; Dragotakes, Q.; Casadevall, A. Variation in cell surface hydrophobicity among *Cryptococcus neoformans* strains influences interactions with amoebas. *mSphere* **2020**, *5*, e00310–e00320. [CrossRef]
19. Scheinpflug, K.; Krylova, O.; Strahl, H. Measurement of cell membrane fluidity by laurdan Gp: Fluorescence spectroscopy and microscopy. *Methods Mol. Biol.* **2017**, *1520*, 159–174. [CrossRef]
20. Vaara, M. Agents that increase the permeability of the outer membrane. *Microbiol. Rev.* **1992**, *56*, 395–411. [CrossRef]
21. Bouyahya, A.; Abrini, J.; Dakka, N.; Bakri, Y. Essential oils of *Origanum compactum* increase membrane permeability, disturb cell membrane integrity, and suppress quorum-sensing phenotype in bacteria. *J. Pharm. Anal.* **2019**, *9*, 301–311. [CrossRef] [PubMed]

22. Singh, N.; Chauhan, A.; Kumar, R.; Singh, S.K. Biochemical and functional characterization of *Mycobacterium tuberculosis* ketol-acid reductoisomerase. *Microbiology* **2021**, *167*, 001087. [[CrossRef](#)] [[PubMed](#)]
23. Yoshida, A.; Yoshida, M.; Kuzuyama, T.; Nishiyama, M.; Kosono, S. Protein acetylation on 2-isopropylmalate synthase from *Thermus thermophilus* Hb27. *Extremophiles* **2019**, *23*, 377–388. [[CrossRef](#)] [[PubMed](#)]
24. Hashiguchi, K.; Kojima, H.; Sato, K.; Sano, K. Effects of an *Escherichia coli* lva mutant gene encoding feedback-resistant threonine deaminase on L-isoleucine production by *Brevibacterium flavum*. *Biosci. Biotechnol. Biochem.* **1997**, *61*, 105–108. [[CrossRef](#)] [[PubMed](#)]
25. Nango, E.; Yamamoto, T.; Kumasaka, T.; Eguchi, T. Crystal structure of 3-isopropylmalate dehydrogenase in complex with NAD<sup>+</sup> and a designed inhibitor. *Bioorg. Med. Chem.* **2009**, *17*, 7789–7794. [[CrossRef](#)] [[PubMed](#)]
26. Lipps, G.; Krauss, G. Adenylosuccinate synthase from *Saccharomyces cerevisiae*: Homologous overexpression, purification and characterization of the recombinant protein. *Biochem. J.* **1999**, *341*, 537–543. [[CrossRef](#)] [[PubMed](#)]
27. Li, Z.; Xu, M.; Wei, H.; Wang, L.; Deng, M. RNA-seq analyses of antibiotic resistance mechanisms in *Serratia marcescens*. *Mol. Med. Rep.* **2019**, *20*, 745–754. [[CrossRef](#)]
28. Pelletier, J.; Thomas, G.; Volarević, S. Ribosome biogenesis in cancer: New players and therapeutic avenues. *Nat. Rev. Cancer* **2018**, *18*, 51–63. [[CrossRef](#)]
29. Wilson, D.N. Ribosome-targeting antibiotics and mechanisms of bacterial resistance. *Nat. Rev. Microbiol.* **2014**, *12*, 35–48. [[CrossRef](#)]
30. Salah Ud-Din, A.I.M.; Roujeinikova, A. Methyl-accepting chemotaxis proteins: A core sensing element in prokaryotes and archaea. *Cell. Mol. Life Sci.* **2017**, *74*, 3293–3303. [[CrossRef](#)]
31. Cooper, K.G.; Chong, A.; Kari, L.; Jeffrey, B.; Starr, T.; Martens, C.; McClurg, M. Regulatory protein HilD stimulates *Salmonella* Typhimurium invasiveness by promoting smooth swimming via the methyl-accepting chemotaxis protein McpC. *Nat. Commun.* **2021**, *12*, 348. [[CrossRef](#)] [[PubMed](#)]
32. Bi, F.; Ma, R.; Ma, S. Discovery and optimization of NAD<sup>+</sup>-dependent DNA ligase inhibitors as novel antibacterial compounds. *Curr. Pharm. Design* **2017**, *23*, 2117–2130. [[CrossRef](#)] [[PubMed](#)]
33. Furman, C.M.; Elbashir, R.; Alani, E. Expanded roles for the MutL family of DNA mismatch repair proteins. *Yeast* **2021**, *38*, 39–53. [[CrossRef](#)] [[PubMed](#)]
34. Yu, L.; Lu, W.; Ye, C.; Wang, Z.; Zhong, M.; Chai, Q.; Sheetz, M.; Wei, Y. Role of a conserved residue R780 in *Escherichia coli* multidrug transporter acrB. *Biochemistry* **2013**, *52*, 6790. [[CrossRef](#)] [[PubMed](#)]
35. Alfonso-Prieto, M.; Biarnés, X.; Vidossich, P.; Rovira, C. The molecular mechanism of the catalase reaction. *J. Am. Chem. Soc.* **2009**, *131*, 11751–117661. [[CrossRef](#)] [[PubMed](#)]
36. Mizrahi Nebenzahl, Y.; Blau, K.; Kushnir, T.; Shagan, M.; Portnoi, M.; Cohen, A.; Azriel, S. *Streptococcus pneumoniae* cell-wall-localized phosphoenolpyruvate protein phosphotransferase can function as an adhesin: Identification of its host target molecules and evaluation of its potential as a vaccine. *PLoS ONE* **2016**, *11*, e0150320. [[CrossRef](#)] [[PubMed](#)]
37. Ito, S.; Koyama, N.; Osanai, T. Citrate synthase from *Synechocystis* is a distinct class of bacterial citrate synthase. *Sci. Rep.* **2019**, *9*, 6038. [[CrossRef](#)]
38. Jung, J.; Lee, S.J. Biochemical and biodiversity insights into heavy metal ion-responsive transcription regulators for synthetic biological heavy metal sensors. *J. Microbiol. Biotechnol.* **2019**, *29*, 1522–1542. [[CrossRef](#)]
39. Groshong, A.M.; McLain, M.A.; Radolf, J.D. Host-specific functional compartmentalization within the oligopeptide transporter during the *Borrelia burgdorferi* enzootic cycle. *PLoS Pathog.* **2021**, *17*, e1009180. [[CrossRef](#)]
40. Li, S.; Wang, L.; Sun, S.; Wu, Q. Hepsin: A multifunctional transmembrane serine protease in pathobiology. *FEBS J.* **2021**, *288*, 5252–5264. [[CrossRef](#)]
41. Tonkin, M.; Khan, S.; Wani, M.Y.; Ahmad, A. QS-a stratagem for conquering multi-drug resistant pathogens. *Curr. Pharm. Design* **2021**, *27*, 2835–2847. [[CrossRef](#)] [[PubMed](#)]
42. Bayaraa, T.; Kurz, J.L.; Patel, K.M.; Hussein, W.M.; Bilyj, J.K.; West, N.P.; Schenk, G.; McGeary, R.P.; Guddat, L.W. Discovery, synthesis and evaluation of a ketol-acid reductoisomerase inhibitor. *Chemistry* **2020**, *26*, 8958–8968. [[CrossRef](#)] [[PubMed](#)]
43. Kim, H.J.; Black, M.; Edwards, R.A.; Peillard-Fiorente, F.; Panigrahi, R.; Klingler, D.; Eidelpes, R. Structural basis for recognition of transcriptional terminator structures by ProQ/FinO domain RNA chaperones. *Nat. Commun.* **2022**, *13*, 7076. [[CrossRef](#)] [[PubMed](#)]
44. Saoud, J.; Mani, T.; Rohrbach, P.; Faucher, S.P. A tail-specific protease is required for *Legionella pneumophila* intracellular multiplication. *Can. J. Microbiol.* **2022**, *68*, 747–757. [[CrossRef](#)] [[PubMed](#)]
45. DeAngelis, C.M.; Nag, D.; Withey, J.H.; Matson, J.S. Characterization of the *Vibrio cholerae* phage shock protein response. *J. Bacteriol.* **2019**, *201*, e0076118. [[CrossRef](#)] [[PubMed](#)]
46. Luckose, F.; Pandey, M.C.; Radhakrishna, K. Effects of amino acid derivatives on physical, mental, and physiological activities. *Crit. Rev. Food Sci. Nutr.* **2015**, *13*, 1793–1807. [[CrossRef](#)] [[PubMed](#)]
47. Li, F.; Fu, T.; Tong, W.D.; Liu, B.H.; Li, C.X.; Gao, Y.; Wu, J.S.; Wang, X.F.; Zhang, A.P. Lubiprostone is effective in the treatment of chronic idiopathic constipation and irritable bowel syndrome: A systematic review and meta-analysis of randomized controlled trials. *Mayo Clin. Proc.* **2022**, *13*, 472. [[CrossRef](#)]
48. Sharma, A.; Biharee, A.; Kumar, A.; Jaitak, V. Antimicrobial terpenoids as a potential substitute in overcoming antimicrobial resistance. *Curr. Drug Targets* **2020**, *21*, 1476–1494. [[CrossRef](#)]

49. Hang, S.; Wu, W.; Wang, Y.; Sheng, R.; Fang, Y.; Guo, R. Daphnetin, a coumarin in genus *Stellera chamaejasme* Linn: Chemistry, bioactivity and therapeutic potential. *Chem. Biodivers.* **2022**, *19*, e202200261. [[CrossRef](#)]
50. Yang, T.; Sun, S.; Wang, T.; Tong, X.; Bi, J.; Wang, Y.; Sun, Z. Piperlonguminine is neuroprotective in experimental rat stroke. *Int. Immunopharmacol.* **2014**, *23*, 447–451. [[CrossRef](#)]
51. Valentová, K.; Vrba, J.; Bancířová, M.; Ulrichová, J.; Křen, V. Isoquercitrin: Pharmacology, toxicology, and metabolism. *Food Chem. Toxicol.* **2014**, *68*, 267–282. [[CrossRef](#)]
52. Cui, J.; Hölzl, G.; Karmainski, T.; Tiso, T.; Kubick, S.I.; Thies, S.; Blank, L.M.; Jaeger, K.E.; Dörmann, P. The glycine-gluco lipid of *alcanivorax borkumensis* is resident to the bacterial cell wall. *Appl. Environ. Microbiol.* **2022**, *88*, e0112622. [[CrossRef](#)]
53. Lin, Z.; Lin, Y.; Zhang, Z.; Shen, J.; Yang, C.; Jiang, M.; Hou, Y. Systematic analysis of bacteriostatic mechanism of flavonoids using transcriptome and its therapeutic effect on vaginitis. *Aging* **2020**, *12*, 6292–6305. [[CrossRef](#)]
54. Atta, S.; Waseem, D.; Fatima, H.; Naz, I.; Rasheed, F.; Kanwal, N. Antibacterial potential and synergistic interaction between natural polyphenolic extracts and synthetic antibiotic on clinical isolates. *Saudi J. Biol. Sci.* **2023**, *30*, 103576. [[CrossRef](#)]
55. Yang, L.; Wang, Y.; Yu, P.; Ren, S.; Zhu, Z.; Jin, Y.; Yan, J.; Peng, X.; Chen, L. Prophage-related gene *Vpachn25\_0724* contributes to cell membrane integrity and growth of *Vibrio parahaemolyticus* Chn25. *Front. Cell. Infect. Microbiol.* **2020**, *10*, 595709. [[CrossRef](#)] [[PubMed](#)]

**Disclaimer/Publisher’s Note:** The statements, opinions and data contained in all publications are solely those of the individual author(s) and contributor(s) and not of MDPI and/or the editor(s). MDPI and/or the editor(s) disclaim responsibility for any injury to people or property resulting from any ideas, methods, instructions or products referred to in the content.